SCIENCE CHINA
Technological Sciences

• Article •

April 2015 Vol.58 No.4: 650–658
doi: 10.1007/s11431-015-5785-4

# Vapor-liquid equilibria of $CH_4$, $CO_2$ and their binary system $CH_4$ + $CO_2$: A comparison between the molecular simulation and equation of state

YANG Zhi[1,2], GONG MaoQiong[1*], ZHOU Yuan[1], DONG XueQiang[1], LI XiaoDong[3], LI HuiYa[1] & WU JianFeng[1]

[1] *Key Laboratory of Cryogenics, Technical Institute of Physics and Chemistry, Chinese Academy of Sciences, Beijing 100190, China;*
[2] *University of Chinese Academy of Sciences, Beijing 100049, China;*
[3] *School of Energy and Power Engineering, Beihang University, Beijing 100191, China*

Received November 15, 2014; accepted February 3, 2015; published online March 9, 2015

An accurate knowledge about phase behaviors of $CH_4$, $CO_2$ and their binary mixture is crucial in fields of natural gas liquefaction and refrigeration applications. In this work, two all-atom force fields of TraPPE-EH and EMP2 were used for the components $CH_4$ and $CO_2$, respectively. Then the vapor-liquid equilibria (VLE) of $CH_4$, $CO_2$ and their binary system were calculated via the NVT- and NpT Gibbs Ensemble Monte Carlo Simulations. Meanwhile the traditional method using Equation of State (EoS) to correlate the VLE properties was also investigated. The EoSs considered in this work were three classic cubic RK, SRK, PR and another advanced molecular-based PC-SAFT equations. For pure components, both molecular simulations and the PC-SAFT EoS could obtain satisfactory predictions for all the saturated properties. However, the saturated liquid densities calculated by the cubic EoSs were not so good. It was also observed that the TraPPE-EH force field had a good representation for $CH_4$ molecule, while the EMP2 force field was not enough accurate to represent $CO_2$ molecules. For the mixture $CH_4$ + $CO_2$, SRK and PR showed the best predictions for the saturated pressure-component property, while good results were also obtained via molecular simulations and PC-SAFT EoS. It was suggested that special combining rules or binary interaction parameters were important to obtain enough accurate prediction of the mixed phase behavior. Compared with the cubic EoS, the PC-SAFT and molecular simulation method showed better adaptabilities for both the pure and mixture systems. Besides, the accurate molecular parameters used in the PC-SAFT and molecular simulations could bring about direct and deep understanding about the molecular characteristics.

**molecular simulation, equation of state, $CH_4$, $CO_2$, vapor-liquid equilibrium**

**Citation:** Yang Z, Gong M Q, Zhou Y, et al. Vapor-liquid equilibria of $CH_4$, $CO_2$ and their binary system $CH_4$+$CO_2$: A comparison between the molecular simulation and equation of state. Sci China Tech Sci, 2015, 58: 650–658, doi: 10.1007/s11431-015-5785-4

## 1 Introduction

Methane ($CH_4$) is the major component of natural gas, which always contains $CO_2$ with various concentrations. For the commercial applications of raw natural gas, a strict pretreatment, namely decarburization and desulfurization or the so-called purification, is always necessary to ensure the production is clean and safe, especially for natural gas liquefaction process [1,2]. They are also important for carbon capture and storage techniques [3,4], the study of flame stabilizing mechanism of methane/air [5,6], and methane recovery from hydrates, which is a promising alternative

*Corresponding author (email: gongmq@mail.ipc.ac.cn)

fossil fuel resource [7,8]. Meanwhile, methane is also found to be used as the refrigerant or one component in the mixed refrigerant for low-temperature refrigeration, e.g. in the three stage cascade refrigeration or mixture refrigeration cycle (MRC) used in the natural gas liquefaction [9,10]. In all the cases, whether the design, optimization of the refrigeration system or the separation, purification processes applied in the natural gas, carbon capture and methane recovery industry, the study of flame mechanism of methane/air, accurate thermophysical data is of crucial importance.

Traditionally, the VLE data are obtained by the experimental method. However, the experimental measurement is expensive and time-consuming. The more efficient methods based on the EoS modeling [11–16] or molecular simulation [17] can also be used to acquire accurate thermophysical properties, which are playing more and more important roles in fields of refrigeration or chemical engineering [18–23]. For EoS modeling, the calculation of the phase behavior is limited by the strong dependence on the experiment and the serious lack of accurate data for the complex fluids. Choosing appropriate EoS to model the special material system is often empirical. However, the recently developed molecular simulation method not only can be used to obtain accurate thermodynamic properties of various materials, but also plays an important role in the extreme conditions [24,25], such as high pressure, toxic, explosive, etc., which are often difficult to be built in the experiment. In addition, with the help of the visualization, the conformational change of the microscopic system can be easily captured, which provides a powerful way to explore the formation mechanism of macroscopic thermodynamic properties [26,27].

Currently, EoS is still the widely used thermodynamic model for the process design. Especially, the classic cubic EoS rooted from van der Waals theory enjoys great popularity in practice for several advantages, such as the simple formation, easy implementation, quick calculation, etc. Among various cubic EoSs, the Redlich-Kwong (RK) [11] is a great breakthrough for the representation of real fluid, while the Soave-Redlich-Kwong (SRK) [12] and Peng-Robinson (PR) [13] make further improvements and have become popular in the industrial applications. Such EoSs are usually of satisfactory accuracy for the simple components including carbon, hydrogen or oxygen atoms, while inaccurate results for liquid densities and large deviations for complex fluids. Recently, the new models based on statistic associating fluid theory [14,15], such as PC-SAFT EoS [16], have attracted much attention [21–23]. Thus, evaluating these EoSs is very helpful to obtaining accurate thermodynamic model for the natural gas constituents.

For molecular simulations, although the simplified force fields could represent pure $CH_4$ and $CO_2$ to a certain extent, the predictions for the mixtures were still not so satisfactory. [28,29] Generally, the all-atom force filed with detailed geometry has better predictions for pure components [30,31], and good results for the mixtures with simple mixing rules [32]. To obtain considerable predictions against the EoS models, two all atom force fields TraPPE-EH [33] and EMP2 [34] were separately used for $CH_4$ and $CO_2$.

In this work, three classic cubic EoSs–namely the RK, PR, and SRK–together with the PC-SAFT were used to calculate the VLE properties of pure components and the mixture involving $CH_4$ and $CO_2$. To obtain accurate representation of the binary system, three different mixing rules were also evaluated. Meanwhile, another promising method, the force-field-based molecular simulation, was also implemented to represent the saturated properties. Finally, a thorough comparison among various EoSs and molecular simulations was presented.

## 2 Equation of state

### 2.1 Cubic EoSs

The cubic EoS, such as RK [11], SRK [12] and PR [13], which can be described with a general formalism [35]:

$$P = \frac{RT}{v-b} - \frac{aa(T)}{v^2 + ubv + wb^2}, \tag{1}$$

where $R$, $a$, $b$ separately denote the universal gas constant; attraction parameter and repulsion parameter or the effective molecular volume. $a(T)$ is a function of temperature, which was introduced for a better correlation to the experimental data ranging from low temperature to the critical point. Different numerical constants of $u$ and $w$ are used to designate different EoSs: $u$=$w$=0 for van der Waals EoS, $u$=1 and $w$=0 for RK and SRK EoS, and $u$=2 and $w$=–1 for PR EoS. Their detailed expressions are listed in Table 1.

As shown in Table 1, parameters $a$ and $b$ used in the cubic EoSs are calculated as a function of critical temperature ($T_c$) and critical pressure ($p_c$). Considering the variations in behavior of different fluids at the same reduced pressure and reduced temperature, the $a(T)$ function of the SRK and PR equations was improved by introducing the acentric factor $\omega$. The values of the desired parameters $T_c$, $p_c$ and $\omega$ for $CH_4$ and $CO_2$ are listed in Table 2.

For the binary system $CH_4$ + $CO_2$, three different mixing rules, van der Waals 1-parameter (VDW1), van der Waals

**Table 1** Expressions of the cubic EoS examined in this work

| EoS | $a$ | $b$ | $a(T)$ |
|---|---|---|---|
| RK | $0.42748 * (R^2(T_c)^{2.5})/P_c$ | $0.08664 * RT_c/P_c$ | $1/(T^{0.5})$ |
| SRK | $0.42748 * (RT_c)^2)/P_c$ | $0.08664 * RT_c/P_c$ | $\left[1+(1-(T_r)^{1/2})(0.48+1.574\omega-0.176\omega^2)\right]^2$ |
| PR | $0.42748 * (RT_c)^2)/P_c$ | $0.07780 * RT_c/P_c$ | $\left[1+(1-(T_r)^{1/2})(0.37464+1.54226\omega-0.26992\omega^2)\right]^2$ |

**Table 2** Critical temperature ($T_c$), critical pressure ($p_c$) and acentric factor ($\omega$) for methane and carbon dioxide

| Component | $T_c$ (K) | $p_c$ (MPa) | $\omega$ |
|---|---|---|---|
| $CH_4$ | 190.60 | 4.61 | 0.0110 |
| $CO_2$ | 304.35 | 7.34 | 0.2236 |

2-parameter (VDW2) and Panagiotopoulos-Reid (P-Reid), were applied.

VDW1 mixing rule:

$$aa(T)=\sum_i\sum_j x_i x_j((a\alpha)_i(a\alpha)_j)^{0.5}(1-k_{ij}), \tag{2}$$

$$b=\sum_i x_i b_i. \tag{3}$$

VDW2 mixing rule:

$$aa(T)=\sum_i\sum_j x_i x_j((a\alpha)_i(a\alpha)_j)^{0.5}(1-k_{ij}), \tag{4}$$

$$b=\sum_i\sum_j x_i x_j b_{ij},\quad \text{where } b_{ij}=\left(\frac{b_i+b_j}{2}\right)\left(1-l_{ij}\right). \tag{5}$$

Panagiotopoulos-Reid mixing rule:

$$aa(T)=\sum_i\sum_j x_i x_j((a\alpha)_i(a\alpha)_j)^{0.5}(1-k_{ij}+\lambda_{ij}x_i), \tag{6}$$

$$b=\sum_i\sum_j x_i x_j b_{ij},\quad \text{where } b_{ij}=\left(\frac{b_i+b_j}{2}\right)\left(1-l_{ij}\right). \tag{7}$$

### 2.2 PC-SAFT EoS

The EoS based on statistic associating fluid theory (SAFT) is being more and more used for the complex systems, such as multi-component, polar and associating fluids [14–16, 36–38], which have gained significant interest by the engineering community.

In this work, one of the most widely used SAFT-tpye EoSs, the Perturbed-Chain Statistical Associating Fluid Theory (PC-SAFT) model [16], was investigated. As a molecule-based EoS, PC-SAFT accounts for the effects of molecular size, molecular shape, dispersion forces and association of molecules. It is based on introducing a defined well model fluid as a reference system and then modeling a real fluid by adding perturbations to the reference system. Lots of good predictions have been obtained for the small molecule, polymer and even complex system [16,38].

The PC-SAFT EoS is written as a summation of the residual Helmholtz free energy terms ($A^{res}$), which correspond to different types of molecular interactions in the system. The residual Helmholtz free energy is equal to the Helmholtz free energy minus the Helmholtz free energy of the ideal gas at the same temperature $T$ and density $\rho$:

$$\begin{aligned}\frac{A^{res}(T,\rho)}{NRT}&=\frac{a^{res}(T,\rho)}{RT}=\frac{a(T,\rho)}{RT}-\frac{a^{ideal}(T,\rho)}{RT}\\&=\frac{a^{ref}(T,\rho)}{RT}+\frac{a^{disp}(T,\rho)}{RT}\\&=\frac{a^{hs}(T,\rho)}{RT}+\frac{a^{chain}(T,\rho)}{RT}+\frac{a^{disp}(T,\rho)}{RT}+\frac{a^{assoc}(T,\rho)}{RT}.\end{aligned} \tag{8}$$

Since no associating interaction exists in $CH_4$ and $CO_2$, only the first three terms and a simple parameter set need to be considered. The parameter set for each pure component consists of three parameters: the number of segments ($m$), segment diameter ($\sigma$), and the energy of dispersion between segments ($\varepsilon/k_b$), which are listed in Table 3.

For the binary mixture $CH_4$ + $CO_2$, dispersion interaction parameters are calculated from the Lorentz–Berthelot combining rules:

$$\sigma_{ij}=\frac{1}{2}\left(\sigma_i+\sigma_j\right), \tag{9}$$

$$\varepsilon_{ij}=\sqrt{\varepsilon_i\varepsilon_j}\left(1-k_{ij}\right). \tag{10}$$

## 3 Molecular simulation

Currently, as an effective complementation to the experiment and semi-empirical correlations, the molecular simulation method is being more and more used to calculate the thermodynamic and phase equilibria properties[17–20,28–32]. However, when applying molecular simulations to represent the real substance, to choose an appropriate potential model or force field is very critical. In this work, two accurate all atom force fields were separately used for $CH_4$ and $CO_2$ to calculate the VLE properties via Gibb ensemble Monte Carlo (GEMC) simulations.

### 3.1 Force fields

The force field was often written as a summation of various contributions, such as the bond stretching, angle bending, dihedral motion or nonbonded interactions. In general, the contributions selected to construct a force field depend on the component of interest. In the past two decades, lots of force fields, such as TraPPE, Amber, Charmm, OPLS force fields[33,40–42], have been developed for various fluids.

These models can be simply divided into three main categories: all-atom (AA), united-atom (UA), or coarse grained (CG) models. Compared with the simplified UA and CG

**Table 3** PC-SAFT parameters [39] for $CH_4$ and $CO_2$

| Component | $m$ | $\sigma$ (Å) | $\varepsilon/k_b$ (K) |
|---|---|---|---|
| $CH_4$ | 1.000 | 3.704 | 150.03 |
| $CO_2$ | 2.6037 | 2.555 | 151.04 |

models, the AA model has a higher or full resolution of the real fluid. For the VLE properties, the main nonbonded Lennard-Jones and electrostatic interactions were considered. Consequently,

$$U_{ij} = \sum_i \sum_j \left\{ 4\varepsilon_{ij} \left[ \left( \frac{\sigma_{ij}}{r_{ij}} \right)^{12} - \left( \frac{\sigma_{ij}}{r_{ij}} \right)^{6} \right] + \frac{q_i q_j}{4\pi\varepsilon_0 r_{ij}} \right\}, \quad (11)$$

where $\varepsilon_0$ is the dielectric constant of the vacuum, $q_i$ is the charge centered on the site of molecule $i$, $r_{ij}$ is the distance between sites $i$ and $j$, $\sigma_{ij}$ and $\varepsilon_{ij}$ separately denote the LJ size and energy parameter between two different sites located at molecules $i$ and $j$.

In this work, two accurate AA models TraPPE-EH [33] and EPM2 [34] for $CH_4$ and $CO_2$ are listed in Table 4.

### 3.2 Simulation details

In molecular simulations, lots of advanced methods, including the Gibbs ensemble Monte Carlo (GEMC) [43], Gibbs Duhem integration [44], *NpT* + test particle [45] and histogram reweighting grand canonical Monte Carlo [46] methods, have been developed for the VLE calculations. In this work, the common GEMC simulation combined with the coupled-decoupled configurational-bias method was employed, which could get rid of the trouble of dealing with the phase surface by dividing the system into two thermodynamic-related phases. As the simulation proceeds, the temperatures, pressures and chemical potential of the two phases or boxes would achieve constant and equal values, i.e. a final phase equilibrium state.

For the pure component, the GEMC method at a constant volume and temperature was adopted to calculate the VLE properties. The simulations were performed for a system of 400 molecules filled in the face centered cubic (fcc) lattice with random orientations. The Ewald sum technique [47] was used to deal with the electrostatic interactions with a cutoff radius adjusted to be half the box length. The cutoff radius for the Lennard-Jones interactions was set to 12 Å, and standard long-range corrections to the energy and pressure were applied. Each simulation was equilibrated for 50000 cycles, followed by production runs of 30000 cycles.

**Table 4** Geometry configurations and potential parameters

| $CH_4$ (TraPPE-EH) | | $CO_2$ (EPM2) | |
|---|---|---|---|
| $r_{C\text{-}H}$ (Å) | 1.10 | $r_{C\text{-}O}$ (Å) | 1.149 |
| $\alpha_{H\text{-}C\text{-}H}$ (eg) | 107.8 | $\alpha_{O\text{-}C\text{-}O}$ (deg) | 180.0 |
| $\sigma_C$ (Å) | 3.31 | $\sigma_C$ (Å) | 2.757 |
| $\sigma_H$ (Å) | 3.46 | $\sigma_O$ (Å) | 3.033 |
| $\varepsilon_C/k_b$ (K) | 0.01 | $\varepsilon_C/k_b$ (K) | 28.129 |
| $\varepsilon_H/k_b$ (K) | 15.30 | $\varepsilon_O/k_b$ (K) | 80.507 |
| $q_C$ | 0.00 | $q_C$ | +0.6512 |
| $q_H$ | 0.00 | $q_O$ | –0.3256 |

Each cycle consisted of 400 attempted moves, such as a volume move, translation of the center of mass, rotation about the center of mass, and a configurational-bias exchange move between two boxes. The moves were selected at random with fixed probabilities.

For the binary system $CH_4$ + $CO_2$, a series of *NpT*-GEMC simulations were performed to calculate the saturated properties (*p*-*T*-*x*-*y*). 500 molecules in total were chosen to construct the fcc lattice. The initial ratio of $CH_4$ to $CO_2$ was 1:1 in each phase. Periodic boundary conditions, Lennard-Jones and electrostatic interactions were set similarly to that of pure component simulations.

## 4 Results and discussion

### 4.1 VLE for pure components

In this work, four EoSs: RK, SRK, PR and PC-SAFT were separately used to calculate the VLE properties of pure $CH_4$ and $CO_2$ in a wide temperature range (from normal boiling point up to the critical point). Figures 1 and 2 show the saturated densities and pressures of $CH_4$, respectively. The saturated densities and pressures of $CO_2$ are respectively shown in Figures 3 and 4. The detailed average absolute relative deviations (AARDs) of pure components are shown in Table 5. The absolute relative deviations of the *NVT*-GEMC simulations are listed in Tables 6 and 7.

As shown in Figures 1–4, all the cubic EoSs gave good accuracies for the vapor densities, while large deviations for the liquid densities. That was maybe due to the too simple attractive terms to describe the condensed liquid state accurately. Meanwhile, since the cubic EoS parameters are functions of the critical properties, an accurate adjustment of the parameter set could ensure their good agreements. However, the parameters of the PC-SAFT EoS were often adjusted by fitting the global experimental data to obtain a smallest

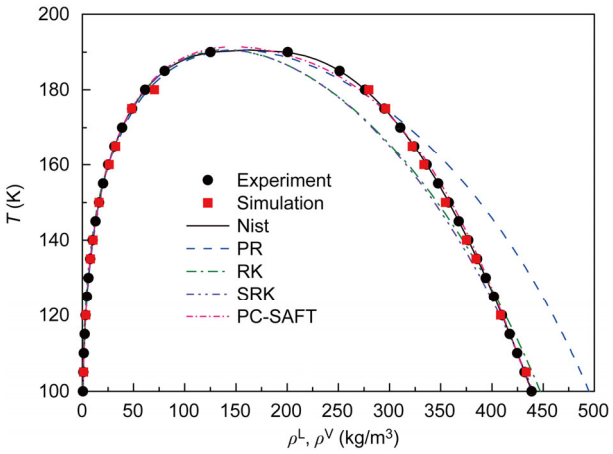


**Figure 1** (Color online) The calculations of the saturated densities for $CH_4$ based on different EoS models and molecular simulations are compared with the reference data (Experiment [48] and NIST [49] data).

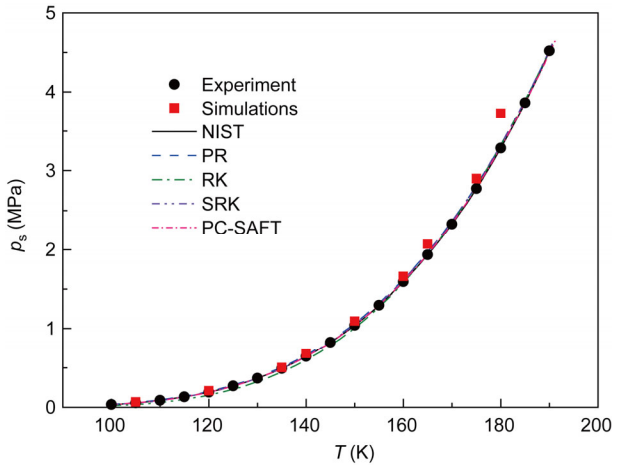


**Figure 2** (Color online) The calculations of the saturated vapor pressure for $CH_4$ based on different EoS models and molecular simulations are compared with the reference data (Experiment [48] and NIST [49] data).

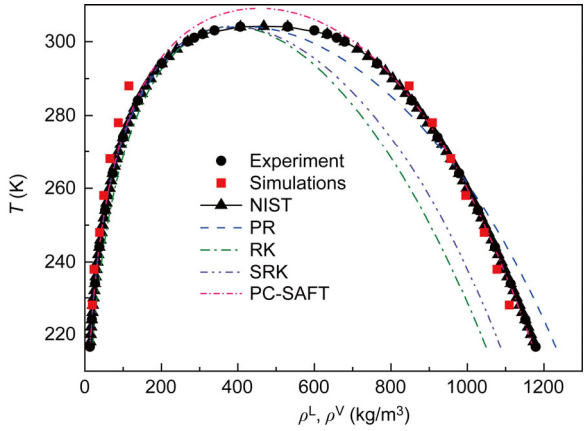


**Figure 3** (Color online) The calculations of the saturated densities for $CO_2$ based on different EoS models and molecular simulations are compared with the reference data (Experiment [50] and NIST [49] data).

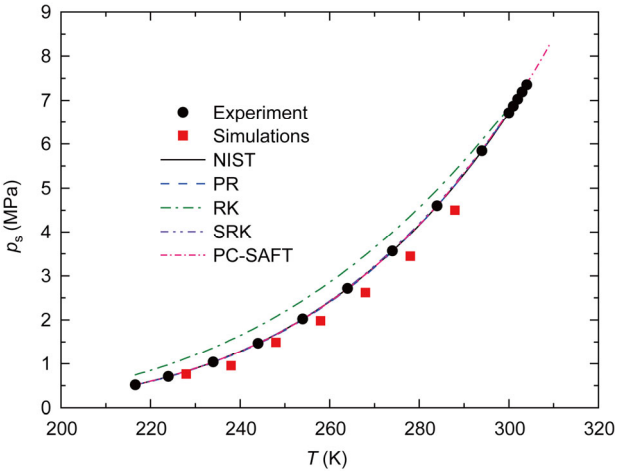


**Figure 4** (Color online) The calculations of the saturated vapor pressure for $CO_2$ based on different EoS models and molecular simulations are compared with the reference data (Experiment [50] and NIST [49] data).

**Table 5** Average absolute relative deviations (AARDs) of the saturated properties between the calculations based on different EoSs and the experiments for pure $CH_4$ and $CO_2$

| Component | Saturated properties | PR | RK | SRK | PC-SAFT |
|---|---|---|---|---|---|
| | | AARDs (%) | | | |
| $CH_4$ $T$=100–190 K | $\rho^V$ | 4.383 | 11.375 | 1.519 | 0.995 |
| | $\rho^L$ | 8.575 | 4.927 | 5.090 | 0.864 |
| | $p_s$ | 3.204 | 10.562 | 1.486 | 0.232 |
| $CO_2$ $T$=217–304 K | $\rho^V$ | 1.205 | 15.739 | 12.207 | 0.386 |
| | $\rho^L$ | 3.973 | 22.567 | 1.234 | 3.158 |
| | $p_s$ | 0.584 | 19.137 | 0.457 | 0.211 |

$\rho^V$, $\rho^L$, $p_s$ separately denote saturated vapor, liquid densities and pressure.

standard deviation. That was why PC-SAFT showed better predictions for the saturated properties in the sub-critical region, but slightly poor predictions for the critical properties. As shown in Table 5, PC-SAFT had the smallest deviations for the saturated properties, while the calculation of RK was poorest because of its simple formation. SRK had a better prediction for $CH_4$ than PR, while a poorer prediction for $CO_2$, which suggests that different EoSs were suitable for different components. Overall, PC-SAFT exhibits better predictions for pure components due to the more flexible parameterization. Besides, the good applications to various substances and clear physical meaning defined by the parameters made the PC-SAFT more attractive and promising.

Where, the average absolute relative deviations (AARDs) were calculated by the following expression:

$$\mathrm{AARD} = \frac{\sum\left|\left(p_{\mathrm{cal}} - p_{\mathrm{exp}}\right)/p_{\mathrm{exp}}\right|}{N} \times 100\%. \qquad (12)$$

For molecular simulations, as shown in Tables 6 and 7, large deviations were obvious near the critical and normal boiling points. That is because the large free energy difference between the gas and liquid phases at low temperatures results cannot reflect the real particle behavior. On the contrary, the particle exchange near the critical point is too frequent to maintain a stationary sate for each of the phases. Thus, both the silent and the frequent particle exchanges

**Table 6** Absolute relative deviations of the saturated properties between molecular simulations and the reference (Experiment [48] or NIST [49] data) for pure $CH_4$

| $T$ (K) | Simulated saturated properties | | | Relative deviations (%) | | |
|---|---|---|---|---|---|---|
| | $P$ (MPa) | $\rho^L$ (kg/m$^3$) | $\rho^V$ (kg/m$^3$) | $\delta p$ | $\delta\rho^L$ | $\delta\rho^V$ |
| 105 | 0.0568 | 433.54 | 1.24 | 16.20 | 0.38 | 10.12 |
| 120 | 0.1943 | 408.45 | 3.35 | 6.54 | 0.35 | 2.70 |
| 135 | 0.4935 | 384.60 | 7.92 | 1.54 | 0.27 | 0.83 |
| 140 | 0.6481 | 375.16 | 10.62 | 5.14 | 0.45 | 4.61 |
| 150 | 1.0780 | 354.67 | 16.54 | 1.41 | 0.90 | 0.75 |
| 160 | 1.5921 | 333.70 | 26.44 | 4.26 | 0.78 | 4.17 |
| 165 | 1.9531 | 322.21 | 32.64 | 5.99 | 0.58 | 3.79 |
| 175 | 2.7865 | 296.30 | 48.20 | 4.04 | 0.46 | 0.74 |
| 180 | 3.3852 | 279.89 | 70.45 | 10.07 | 1.32 | 13.79 |

**Table 7** Absolute relative deviations of the saturated properties between molecular simulations and the reference (Experiment [50] or NIST [49] data) for pure $CO_2$

| $T$ (K) | Simulated saturated properties | | | Relative deviations (%) | | |
|---|---|---|---|---|---|---|
| | $P$ (MPa) | $\rho^L$ (kg/m$^3$) | $\rho^V$ (kg/m$^3$) | $\delta p$ | $\delta\rho^L$ | $\delta\rho^V$ |
| 228 | 0.76 | 1109.60 | 19.68 | 7.32 | 2.23 | 9.72 |
| 238 | 0.98 | 1077.47 | 26.42 | 17.65 | 1.59 | 15.32 |
| 248 | 1.49 | 1044.03 | 38.53 | 10.24 | 0.81 | 11.76 |
| 258 | 1.98 | 996.06 | 49.54 | 12.39 | 1.00 | 17.71 |
| 268 | 2.62 | 956.46 | 65.81 | 12.96 | 0.00 | 20.14 |
| 278 | 3.44 | 908.93 | 87.81 | 12.24 | 1.16 | 23.45 |
| 288 | 4.50 | 847.77 | 115.09 | 10.36 | 2.83 | 28.38 |

would result in large deviations or wrong statistics. In general, the critical properties of the different components were obtained by fitting the simulation results at subcritical conditions to the scaling law [51] and the law of rectilinear diameters [52]. The critical pressures were estimated by extrapolating the vapor pressure curves using the Clausius-Clapeyron equation. This also yielded an estimate of the normal boiling point of the compounds.

As shown in Figures 1 and 2, except for the predictions near the critical and normal boiling points, all the simulated results for the pure $CH_4$ showed good agreements with the reference data [48,49]. The deviations of the saturated vapor density and pressure were slightly large, which could be attributed to the small value of the vapor density and the large fluctuation of the vapor pressure. The predictions of the saturated liquid densities gave the best accuracies. The saturated densities and vapor pressures for the pure $CO_2$ are shown in Figures 3 and 4, respectively. Although the results over the whole temperature range agreed with the reference data [49,50], the saturated vapor densities and vapor pressure showed relatively large deviations compared with that of $CH_4$, which proved that the EMP2 force field was still not enough accurate to describe the complex interactions of $CO_2$ molecules. However, the predictions of the saturated liquid densities were satisfactory.

### 4.2 VLE for binary system $CH_4 + CO_2$

For the binary system $CH_4 + CO_2$, the standard van de Waals mixing rules combined with a simple binary interaction parameter (ie. VDW1) together with another two mixing rules-VDW2 and P-Reid, were used for the cubic EoS modeling, while the Lorentz-Berthelot 1-parameter combining rule was used for PC-SAFT EoS. Then only the binary interaction parameters for each component needed to be adjusted to represent the experiment. The final optimized binary interaction parameters for all the EoSs are listed in Table 8. The comparisons of the VLE properties between the calculations and the experimental data [53,54] at the temperature 230 K are shown in Figure 5, while that at 250 K is shown in Figure 6. The absolute relative deviations of saturated properties are listed in Table 9. Except for the RK EoS, the other three EoSs could represent the real system with relatively small deviations. Different from the pure components, the classic cubic EoSs PR and SRK exhibited better fittings to the experiments than the PC-SAFT. This may be caused by the overestimations of near-critical properties for the pure component. However, when the pressure was below 5 MPa, the calculations of the PC- SAFT showed considerable precisions with that of the PR and SRK EoS. It was also obvious that the predictions at 230 K showed better agreements for all the EoSs than that at 250 K.

**Table 8** The optimized binary interaction parameters for the four EoSs

| EoS | Mixing rule | $k_{ij}$ | $l_{ij}$ | $\lambda_{ij}$ |
|---|---|---|---|---|
| | | $T$=230 K | | |
| RK | VDW1 | 0.12310 | – | – |
| | VDW2 | 0.13910 | 0.06270 | – |
| | P-Reid | 0.41609 | 0.29801 | 0.24022 |
| PR | VDW1 | 0.09549 | – | – |
| | VDW2 | 0.08171 | –0.02775 | – |
| | P-Reid | 0.06615 | –0.04114 | –0.01362 |
| SRK | VDW1 | 0.09825 | – | – |
| | VDW2 | 0.08728 | –0.02255 | – |
| | P-Reid | 0.03650 | –0.06577 | –0.04663 |
| PC-SAFT | L-B | 0.05847 | – | – |
| | | $T$=250 K | | |
| RK | VDW1 | 0.10764 | – | – |
| | VDW2 | 0.16646 | 0.10302 | – |
| | P-Reid | 0.29615 | 0.21618 | 0.14117 |
| PR | VDW1 | 0.10977 | – | – |
| | VDW2 | 0.06825 | –0.05322 | – |
| | P-Reid | 0.03899 | –0.07940 | –0.03218 |
| SRK | VDW1 | 0.10963 | – | – |
| | VDW2 | 0.07941 | –0.04004 | |
| | P-Reid | 0.41609 | 0.29801 | 0.24022 |
| PC-SAFT | L-B | 0.06777 | – | – |

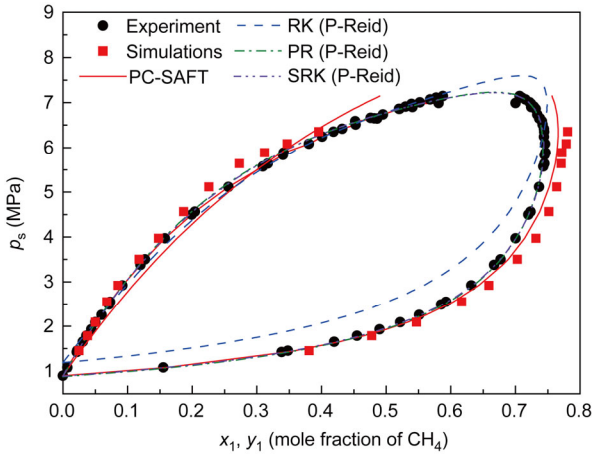


**Figure 5** (Color online) 230 K, mole fractions of $CH_4$ in both phases calculated by different EoS models and molecular simulation were compared with the experiment.

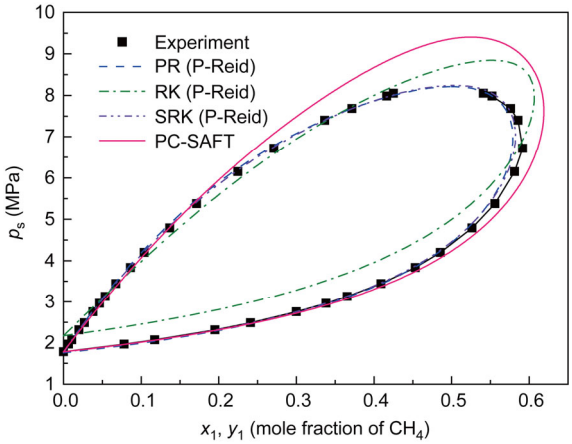


**Figure 6** (Color online) 250 K, mole fractions of $CH_4$ in both phases calculated by different EoS models were compared with the experiment.

**Table 9** Average absolute relative deviations (AARDs) of the saturated properties for the binary system between the calculations based on different EoSs and the experiment

| EoS | Mixing rule | 230 K (AARDs %) | | 250 K (AARDs %) | |
|---|---|---|---|---|---|
| | | $p_s$ | $y_1$ | $p_s$ | $y_1$ |
| RK | VDW1 | 5.4998 | 11.7996 | 6.2545 | 16.8185 |
| | VDW2 | 4.8744 | 13.0234 | 5.5696 | 18.9133 |
| | P-Reid | 3.5823 | 9.9404 | 5.3972 | 17.7862 |
| PR | VDW1 | 2.9675 | 1.7850 | 2.1546 | 1.8647 |
| | VDW2 | 1.0348 | 0.5816 | 1.1219 | 2.2791 |
| | P-Reid | 0.9942 | 0.5068 | 1.0168 | 1.9781 |
| SRK | VDW1 | 2.3554 | 1.8167 | 1.3825 | 2.2510 |
| | VDW2 | 0.9777 | 0.7317 | 0.6549 | 1.4368 |
| | P-Reid | 0.8525 | 0.3551 | 0.4095 | 0.8510 |
| PC-SAFT | L-B1 | 6.3561 | 3.8155 | 3.4859 | 3.8756 |

$p_s$, $y_1$ separately denote the saturated pressure and the vapor mole fraction of $CH_4$.

Among the different mixing rules, the P-Reid best represents the VLE property, while VDW2 better represents the saturated pressure than VDW1. That is because 3 adjustable parameters are contained in the P-Ried mixing rule, while 2 parameters for VDW2 and 1 parameter for VDW1. It suggested that special combining rules or binary interaction parameters were important to obtain enough accurate prediction of the mixed phase behavior.

In addition, the VLE property of the binary system $CH_4$ + $CO_2$ at 230 K was also calculated by the *NpT*-GEMC molecular simulation method, as listed in Table 10. The relations between pressure and mole fraction of $CH_4$ ($p$-$x_1$-$y_1$) are plotted in Figure 4. It was observed that the mole fractions in the vapor phase over the whole pressure range were slightly larger than the experimental data, while the liquid mole fractions were smaller. In addition, when the pressure increased to a certain value, the liquid mole fraction started to approach the experimental points, while the vapor mole fraction was generally away from them. With the increase of pressure, the smaller free energy difference between vapor and liquid phases resulted in a more frequent and sufficient particle exchange, which brought about a larger fluctuation of the particle number in the liquid phase at the same pressure interval. The adopted Lorentz-Berthelot rule was also too simple to represent the mixed characteristic of $CH_4$ and $CO_2$ accurately. However, these deviations could be overcome by introducing special combining rules or binary interaction parameters [55,56].

**Table 10** Comparisons of the saturated properties between molecular simulation and the experiment [48,49] at 230 K

| $P$ (MPa) | $x^{cal}$ | $x^{exp}$ | $y^{cal}$ | $y^{exp}$ |
|---|---|---|---|---|
| 0.892 | – | 0.0000 | – | 0.0000 |
| 0.88 | | 0.00 | | 0.00 |
| 1.078 | – | 0.0070 | – | 0.1553 |
| 1.453 | 0.025 | 0.0221 | 0.402 | 0.3480 |
| 1.500 | | 0.027 | | 0.399 |
| 1.786 | 0.038 | 0.0365 | 0.496 | 0.4550 |
| 2.000 | | 0.050 | | 0.525 |
| 2.092 | 0.050 | 0.0503 | 0.556 | 0.5220 |
| 2.551 | 0.068 | 0.0730 | 0.617 | 0.5930 |
| 2.916 | 0.085 | 0.0920 | 0.659 | 0.6320 |
| 3.200 | 0.102 | 0.115 | 0.677 | 0.683 |
| 3.503 | 0.118 | 0.1269 | 0.703 | 0.6770 |
| 3.968 | 0.156 | 0.1577 | 0.732 | 0.7005 |
| 4.000 | | 0.170 | | 0.728 |
| 4.565 | 0.192 | 0.2042 | 0.758 | 0.7237 |
| 4.800 | 0.206 | 0.235 | 0.760 | 0.751 |
| 5.116 | 0.226 | 0.2560 | 0.762 | 0.7369 |
| 5.500 | 0.240 | 0.318 | 0.768 | 0.764 |
| 5.640 | 0.265 | 0.3171 | 0.771 | 0.7449 |
| 5.885 | 0.302 | 0.3416 | 0.775 | 0.7466 |
| 6.086 | 0.347 | 0.3805 | 0.780 | 0.7461 |
| 6.200 | 0.368 | 0.394 | 0.784 | 0.762 |
| 6.353 | 0.396 | 0.4187 | 0.786 | 0.7448 |

$x^{cal}$, $y^{cal}$ separately denote the vapor and liquid mole fractions of $CH_4$, the superscript "exp" represent the experimental mole fractions.

## 5 Conclusion

In this work, the capabilities of four different EoSs, namely RK, PR, SRK and PC-SAFT, and molecular simulation method were evaluated by calculating the VLE properties of pure components and the binary mixture involving the important industrial components $CH_4$ and $CO_2$.

The cubic EoSs repeated the critical properties very well, while they could not ensure satisfactory precision over the whole temperature range, especially in the liquid phase region. PC-SAFT obtained a better fitting over the whole temperature range, while often overestimated the critical properties. In addition, different cubic EoSs show different adaptabilities, e.g. SRK was more suitable for $CH_4$, while PR for $CO_2$. For the mixture $CH_4$ + $CO_2$, different mixing rules were also evaluated. The P-Reid rules best represented the VLE for the most adjustable parameters. When the rule was given, PR and SRK showed better predictions than

PC-SAFT. However, when the pressure was below 5 MPa, the calculations of PC-SAFT show considerable precisions with that of PR and SRK. The comprehensive comparison suggests that PC-SAFT had a better adaptability for various systems.

In this work, the all-atom force fields were used to calculate the VLE properties. Good agreements were obtained for both the pure component and binary systems. For pure $CO_2$, the saturated vapor densities and pressures seemed to be underestimated because of the simplified EPM2 model, while the TraPPE-EH model for $CH_4$ satisfactorily represented the experimental data. The relatively large deviations near the normal boiling and critical point were mainly caused by the too silent or frequent particle exchange between two phases. For the mixture, the predictions of vapor mole fractions were slightly overestimated over the whole pressure range, while the simulated liquid mole fractions were smaller than the experimental data. When the pressure increased to a certain value, the gas mole fraction began to approach the experimental data, while the liquid mole fractions got far away. Maybe the adopted L-B mixing rule was too simple to reflect the mixed behavior exactly. The correction by introducing special binary interaction parameters or combining rules was significant for molecular simulations to obtain accurate predictions of the mixture.

Both the EoS modeling and molecular simulations are attractive for the calculations of thermodynamic properties. For the EoS method, although the strong dependence on the experimental data makes it difficult to predict the properties beyond the experimental conditions and apply to various systems, the simple formations, fewer parameters and fast calculations have won large popularity in engineering practices. The PC-SAFT and molecular simulations as recently developed methods, have shown good adaptabilities for both pure components and the mixture. Besides, their accurate molecular parameters could bring about direct and deep understanding about the molecular characteristics.

*This work was supported by the National Natural Science Foundation of China (Grant No. 51376188) and the National Basic Research Program of China ("973" Project) (Grant No.2011CB710701).*

1 Kosseim A. New development in gas purification for LNG plants. In: Tenth International Conference & Exhibition on Liquefied Natural Gas, 1992
2 Cao W S. Study on natural gas purification and liquefaction process of small scale LNG project. Dissertation of Doctor Degree. Shanghai: Shanghai Jiaotong University, 2008
3 Oldenburg C M, Pruess K, Benson S M. Process modeling of $CO_2$ injection into natural gas reservoirs for carbon sequestration and enhanced gas recovery. Energy Fuels, 2001, 15: 293–298
4 Class H, Ebigbo A, Helmig R, et al. A benchmark study on problems related to $CO_2$ storage in geologic formations. Comput Geosci, 2009, 13: 409–434
5 Han C, Zhang P, Ye T H, et al. Numerical study of methane/air jet flame in vitiated co-flow using tabulated detailed chemistry. Sci China Tech Sci, 2014, 57: 1750–1760
6 Yu J, Meng H. A numerical study of counterflow diffusion flames of methane/air at various pressures. Sci China Tech Sci, 2014, 57: 615–624
7 Kvenvolden K A. Gas hydrates-geological perspective and global change. Rev Geophys, 1993, 31: 173–187
8 Deusner C, Bigalke N, Kossel E, et al. Methane production from gas hydrate deposits through injection of supercritical $CO_2$. Energies, 2012, 5: 2112–2140
9 Kanoğlu M. Exergy analysis of multistage cascade refrigeration cycle used for natural gas liquefaction. Int J Energ Res, 2002, 26: 763–774
10 Lim W, Choi K, Moon I. Current status and perspectives of liquefied natural gas (LNG) plant design. Ind Eng Chem Res, 2013, 52: 3065–3088
11 Redlich O, Kwong J N S. On the thermodynamics of solutions. V. An equation of state. Fugacities of gaseous solutions. Chem Rev, 1949, 44: 233–244
12 Soave, G. Equilibrium constants from a modified Redlich–Kwong equation of state. Chem Eng Sci, 1972, 27: 1197–1203
13 Peng D Y, Robinson D B. A new two-constant equation of state. Ind Eng Chem Fundam, 1976, 15: 59–64
14 Chapman W G, Gubbins K E, Jackson G, et al. SAFT: Equation-of-state solution model for associating fluids. Fluid Phase Equilib, 1989, 52: 31–38
15 Huang S H, Radosz M. Equation of state for small, large, polydisperse, and associating molecules. Ind Eng Chem Res, 1990, 29: 2284–2294
16 Gross J, Sadowski G. Perturbed-chain SAFT: An equation of state based on a perturbation theory for chain molecules. Ind Eng Chem Res, 2001, 40: 1244–1260
17 Panagiotopoulos A Z. Direct determination of fluid phase equilibria by simulation in the Gibbs ensemble: A review. Mol Sim, 1992, 9: 1–23
18 Skvorova M, Smith W R. Molecular-level simulation of bubble and dew points of fluid mixtures and application to refrigerant cycle design. Int J Refrig, 2014, 42: 1–7
19 Smith W R, Figueroa-Gerstenmaier S, Skvorova M. Molecular simulation for thermodynamic properties and process modeling of refrigerants. J Chem Engin Data, 2014, 59: 3258–3271
20 Figueroa-Gerstenmaier S, Lísal M, Nezbeda I, et al. Prediction of isoenthalps, Joule–Thomson Coefficients and Joule–Thomson inversion curves of refrigerants by molecular simulation Fluid Phase Equilibr, 2014, 375: 143–151
21 Vinš V, Hrubý J. Solubility of nitrogen in one-component refrigerants: Prediction by PC-SAFT EoS and a correlation of Henry's law constants. Int J Refrig, 2011, 34: 2109–2117
22 Marcelino Neto M A, Barbosa Jr J R. Prediction of refrigerant-lubricant viscosity using the general PC-SAFT friction theory. Int J Refrig, 2014, 45: 92–99
23 Polishuk I, Assor E, Cohen N, et al. Implementation of PC-SAFT and SAFT+ Cubic for modeling thermodynamic properties of haloalkanes. II. 7 Haloethanes and their mixtures. Int J Refrig, 2013, 36: 980–991
24 Liu Y, Panagiotopoulos A Z, Debenedetti P G. Monte carlo simulations of high-pressure phase equilibria of $CO_2$–$H_2O$ mixtures. J Phys Chem B, 2011, 115: 6629–6635
25 Lin W, Yang Q, Zhong C. Molecular simulation of vapor–liquid equilibria of toxic gases. Fluid Phase Equilibr, 2004, 220: 1–6
26 Do H, Wheatley R J, Hirst J D. Microscopic structure of liquid 1-1-1-2-tetrafluoroethane (R134a) from Monte Carlo simulation. Phys Chem Chem Phys, 2010, 12: 13266–13272
27 Yamakov V, Wolf D, Phillpot S R, et al. Deformation-mechanism map for nanocrystalline metals by molecular-dynamics simulation. Nat Mater, 2003, 3: 43–47
28 Vrabec J, Fischer J. Vapor-liquid equilibria of binary mixtures containing methane, ethane, and carbon dioxide from molecular simulation. Int J Thermophys, 1996, 17: 889–908
29 Liu A, Beck T L. Vapor-liquid equilibria of binary and ternary mixtures containing methane, ethane, and carbon dioxide from Gibbs ensemble simulations. J Phys Chem B, 1998, 102: 7627–7631

30 Peguin R P S, Kamath G, Potoff J J, et al. All-atom force field for the prediction of vapor–liquid equilibria and interfacial properties of HFA134a. J Phys Chem B, 2008, 113: 178–187
31 Raabe G, Maginn E J. A force field for 3, 3, 3-fluoro-1-propenes, including HFO-1234yf. J Phys Chem B, 2010, 114: 10133–10142
32 Raabe G. Molecular simulation studies on the vapor–liquid phase equilibria of binary mixtures of R-1234yf and R-1234ze (E) with R-32 and $CO_2$. J Chem Engin Data, 2013, 58: 1867–1873
33 Chen B, Siepmann J I. Transferable potentials for phase equilibria. 3. Explicit-hydrogen description of normal alkanes. J Phys Chem B, 1999, 103: 5370–5379
34 Harris J G, Yung K H. Carbon dioxide's liquid-vapor coexistence curve and critical properties as predicted by a simple molecular model. J Phys Chem, 1995, 99: 12021–12024
35 Daridon J L, Saint-Guirons H, La Courette B, et al. A generalized process for phase equilibrium calculation with cubic equations of state. Int J Thermophys, 1993, 14: 1101–1108
36 Grandjean L, de Hemptinne J C, Lugo R. Application of GC-PPC-SAFT EoS to ammonia and its mixtures. Fluid Phase Equilibr, 2014, 367: 159–172
37 NguyenHuynh D, Passarello J P, Tobaly P, et al. Application of GC-SAFT EOS to polar systems using a segment approach. Fluid Phase Equilibr, 2008, 264: 62–75
38 Gross J, Sadowski G. Application of the perturbed-chain SAFT equation of state to associating systems. Ind Eng Chem Res, 2002, 41: 5510–5515
39 Diamantonis N I, Economou I G. Evaluation of statistical associating fluid theory (SAFT) and perturbed Chain-SAFT equations of state for the calculation of thermodynamic derivative properties of fluids related to carbon capture and sequestration. Energy Fuels, 2011, 25: 3334–3343
40 Cornell W D, Cieplak P, Bayly C I, et al. A second generation force field for the simulation of proteins, nucleic acids, and organic molecules. J Am Chem Soc, 1995, 117: 5179–5197
41 MacKerell A D, Bashford D, Bellott M, et al. All-atom empirical potential for molecular modeling and dynamics studies of proteins. J Phys Chem B, 1998, 102: 3586–3616
42 Jorgensen W L, Maxwell D S, Tirado-Rives J. Development and testing of the OPLS all-atom force field on conformational energetics and properties of organic liquids. J Am Chem Soc, 1996, 118: 11225–11236
43 Panagiotopoulos A Z. Direct determination of phase coexistence properties of fluids by Monte Carlo simulation in a new ensemble. Mol Phys, 1987, 61: 813–826
44 Kofke D A. Direct evaluation of phase coexistence by molecular simulation via integration along the saturation line. J Chem Phys, 1993, 98: 4149–4162
45 Vrabec J, Stoll J, Hasse H. A set of molecular models for symmetric quadrupolar fluids. J Phys Chem B, 2001, 105: 12126–12133
46 Potoff J J, Panagiotopoulos A Z. Critical point and phase behavior of the pure fluid and a Lennard-Jones mixture. J Chem Phys, 1998, 109: 10914–10920
47 Allen M P, Tildesley D J. Computer Simulation of Liquids. Oxford: Clarendon, 1987
48 Kleinrahm R, Wagner W. Measurement and correlation of the equilibrium liquid and vapour densities and the vapour pressure along the coexistence curve of methane. J Chem Thermodyn, 1986, 18: 739–760
49 Lemmon E W, Huber M L, McLinden M O. 2007, NIST Reference Fluid Thermodynamic and Transport Properties-REFPROP, NIST Standard Reference Database 23-Version 8.0
50 Duschek W, Kleinrahm R, Wagner W. Measurement and correlation of the (pressure, density, temperature) relation of carbon dioxide II. Saturated-liquid and saturated-vapour densities and the vapour pressure along the entire coexistence curve. J Chem Thermodyn, 1990, 22: 841–864
51 Rowlinson J S, Swinton F L. Liquids and Liquid Mixtures. 3rd ed. London: Butterworth, 1982
52 Rowlinson J S, Widom B. Molecular Theory of Capillarity. Oxford: Clarendon Press, 1982
53 Davalos J, Anderson W R, Phelps R E, et al. Liquid-vapor equilibria at 250.00. deg. K for systems containing methane, ethane, and carbon dioxide. J Chem Eng Data, 1976, 21: 81–84
54 Wei M S W, Brown T S, Kidnay A J, et al. Vapor+ liquid equilibria for the ternary system methane+ ethane+ carbon dioxide at 230 K and its constituent binaries at temperatures from 207 to 270 K. J Chem Eng Data, 1995, 40: 726–731
55 Vrabec J, Stoll J, Hasse H. Molecular models of unlike interactions in fluid mixtures. Mol Sim, 2005, 31: 215–221
56 Schnabel T, Vrabec J, Hasse H. Unlike Lennard–Jones parameters for vapor–liquid equilibria. Mol Liq, 2007, 135: 170–178